Article

TRANSPARENT PROCESS

THE EMBO JOURNAL

Crosstalk between Akt/GSK3β signaling and dynamin-1 regulates clathrin-mediated endocytosis

Carlos R Reis[1,†], Ping-Hung Chen[1,†], Saipraveen Srinivasan[1], François Aguet[2], Marcel Mettlen[1] & Sandra L Schmid[1,*]

Abstract

Clathrin-mediated endocytosis (CME) regulates signaling from the plasma membrane. Analysis of clathrin-coated pit (CCP) dynamics led us to propose the existence of a rate-limiting, regulatory step(s) that monitor the fidelity of early stages in CCP maturation. Here we show that nascent endocytic vesicles formed in mutant cells displaying rapid, dysregulated CME are defective in early endosomal trafficking, maturation and acidification, confirming the importance of this "checkpoint." Dysregulated CME also alters EGF receptor signaling and leads to constitutive activation of the protein kinase Akt. Dynamin-1, which was thought to be neuron specific, is activated by the Akt/GSK3β signaling cascade in non-neuronal cells to trigger rapid, dysregulated CME. Acute activation of dynamin-1 in RPE cells by inhibition of GSK3β accelerates CME, alters CCP dynamics and, unexpectedly, increases the rate of CCP initiation. CRISPR-Cas9n-mediated knockout and reconstitution studies establish that dynamin-1 is activated by Akt/GSK3β signaling in H1299 non-small lung cancer cells. These findings provide direct evidence for an isoform-specific role for dynamin in regulating CME and reveal a feed-forward pathway that could link signaling from cell surface receptors to the regulation of CME.

Keywords CME; endosomal trafficking; signaling; dynamin; CCP maturation
Subject Categories Membrane & Intracellular Transport
DOI 10.15252/embj.201591518 | Received 13 March 2015 | Revised 26 May 2015 | Accepted 10 June 2015 | Published online 2 July 2015
The EMBO Journal (2015) 34: 2132–2146

Introduction

Clathrin-mediated endocytosis (CME) constitutes the major entry pathway for signaling receptors, transporters and adhesion molecules into eukaryotic cells (Traub, 2009; McMahon & Boucrot, 2011; Ferguson & De Camilli, 2012). CME is a multi-step process involving the formation, stabilization and maturation of clathrin-coated pits (CCPs), leading to the incorporation of surface receptors and their ligands into clathrin-coated vesicles (CCVs). During CCP maturation, the CME core machinery consisting of clathrin, dynamin and AP2 interacts with a myriad of endocytic accessory proteins (EAPs), many of which are recruited to CCPs via binding to the appendage domain (AD) of the α-adaptin subunit of AP2 (Schmid & McMahon, 2007). Following maturation, membrane scission is catalyzed by the GTPase dynamin, leading to the formation of cargo-containing vesicles.

Although the endocytic machinery is well understood, many questions remain as to how CME is regulated. Analyses of CCP dynamics by live cell imaging revealed striking differences in their assembly and maturation kinetics, including the existence of short-lived, abortive CCPs (Ehrlich *et al*, 2004; Loerke *et al*, 2009; Taylor *et al*, 2012) and early rate-limiting step(s) required to monitor the fidelity of CCP maturation (Aguet *et al*, 2013). The manipulation of cargo concentration (Loerke *et al*, 2009), the induction of receptor clustering (Liu *et al*, 2010), as well as small interfering RNA (siRNA) knockdown of a subset of EAPs (Mettlen *et al*, 2009b) shifted the relative proportions of abortive vs. productive CCPs and/or altered the lifetimes of abortive CCPs. In addition to establishing a role for these factors in CCP maturation, these findings led to the hypothesis that transitions leading to the formation of mature CCPs are gated by a checkpoint mechanism(s) that monitors coat assembly, cargo recruitment and membrane curvature (Mettlen *et al*, 2009a). While still controversial (McMahon & Boucrot, 2011; Ferguson & De Camilli, 2012), the strongest evidence for the existence of an endocytic checkpoint derives from recent observations of the rapid and active turnover of aberrant flat clathrin lattices that formed in cells expressing a truncated α-adaptin subunit lacking the AD (ΔαAD) (Aguet *et al*, 2013). Despite their severe defect in early stages of CCP maturation, the rate of TfnR uptake in these cells is unimpaired due to two compensatory mechanisms. First, the rate of CCP initiation doubles, and second, those CCPs able to bypass the endocytic checkpoint undergo a more rapid and dysregulated maturation. Thus, these cells represent a powerful tool to study the regulation of CME.

Clathrin-mediated endocytosis regulation is important because cell surface signaling is governed by endocytic trafficking, either by the rapid clearance of surface receptors leading to the attenuation of incoming signals or by the formation of endosome-specific signal

1 Department of Cell Biology, UT Southwestern Medical Center, Dallas, TX, USA
2 Department of Cell Biology, Harvard Medical School, Boston, MA, USA
*Corresponding author. Tel: +1 214 648 3948; E-mail: Sandra.Schmid@utsouthwestern.edu
†These authors contributed equally to this work

transduction complexes (Schenck *et al*, 2008; Sorkin & von Zastrow, 2009; Zoncu *et al*, 2009; Platta & Stenmark, 2011; Palfy *et al*, 2012). Indeed, a recently generated hierarchical map of endocytic membrane trafficking has revealed close interactions between signaling and endocytic pathways (Liberali *et al*, 2014), which remain unexplored.

The GTPase dynamin, which assembles into a fission apparatus at the necks of deeply invaginated CCPs, has been proposed to also function as a regulator of early, rate-limiting steps in CCV formation (Sever *et al*, 1999; Loerke *et al*, 2009; Aguet *et al*, 2013). There are three major mammalian isoforms: dynamin-1 (Dyn1), which is presumed to be neuron specific; dynamin-2 (Dyn2), which is ubiquitously expressed; and dynamin-3 (Dyn3), mainly expressed in testis, brain and lung. Although sharing significant sequence identity, Dyn1 and Dyn2 differ in their curvature-generating/sensing properties (Liu *et al*, 2011). It has been proposed that Dyn1, which has more potent curvature-generating properties, is suited for rapid, compensatory endocytosis at the synapse, whereas the curvature-sensing properties of Dyn2, which requires a narrow neck to trigger its assembly, are suited to monitor and regulate early stages of CCP maturation (Liu *et al*, 2011). Indeed, there is evidence for isoform-specific functions of Dyn1 and Dyn2 in CME both at the synapse (Ferguson *et al*, 2007) and in non-neuronal cells (Liu *et al*, 2008), respectively. However, the basis for these differences and their functional significance remains poorly understood.

Through mechanistic studies of endocytosis in cells defective in early stages of CCP maturation, we have discovered an endosome-associated signaling pathway that activates endogenously expressed but normally quiescent dynamin-1 in non-neuronal cells. This signaling pathway exists in normal RPE cells and is activated in the non-small cell lung cancer cell line, H1299. Acute activation of dynamin-1 increases the rate of CCP initiation, alters CCP dynamics and triggers rapid, dysregulated CME. These data establish an isoform-specific role for dynamin in regulating early stages of CME and point to the existence of a two-way crosstalk between signaling and CME.

Results

Dysregulated CME produces nascent CCVs defective in endosomal trafficking and maturation

Despite being severely defective in the early stages of CCP maturation (Aguet *et al*, 2013), the rate of Tfn uptake in ΔαAD cells is unaffected (Motley *et al*, 2006; Aguet *et al*, 2013). We first confirmed that the compensatory endocytosis leading to efficient TfnR uptake was clathrin dependent (Supplementary Fig S1A) and that the steady-state levels of surface TfnR remained unaffected in control and ΔαAD cells (Supplementary Fig S1B). Thus, although an operational checkpoint in these cells rapidly turns over the majority of aberrant CCPs, we proposed that a subset of productive CCPs mature in a more rapid and dysregulated manner, as a result of bypassing the endocytic checkpoint (Aguet *et al*, 2013). Although best understood in the context of cell division, by definition checkpoints function as fidelity monitors to ensure the accuracy of the molecular events being monitored. If a subset of CCVs formed in ΔαAD cells had indeed bypassed this regulatory step(s), then they should exhibit defects that would have functional consequences for their downstream processing. We tested this hypothesis by comparing early endosomal trafficking in control cells reconstituted with full-length α-adaptin (FL cells) and ΔαAD cells.

Newly formed nascent endocytic vesicles undergo multiple rounds of homotypic and heterotypic fusion at the cell periphery, driving the maturation of larger early endosomes that then move toward the perinuclear region (Gorvel *et al*, 1991; Rink *et al*, 2005). Early endosomes undergo acidification and mediate the sorting of selective cargos for recycling and/or degradation (Mellman, 1996; Maxfield & McGraw, 2004; Grant & Donaldson, 2009). We first examined the trafficking of labeled transferrin (Tfn) through early endosomes by incubating both FL and ΔαAD cells with a brief (2-min) pulse of Tfn-AlexaFluor®647 (Tfn^{AF647}), followed by a second 2-min pulse with Tfn-AlexaFluor®568 (Tfn^{AF568}). As expected (Fig 1A, top panel), rapid homo- and heterotypic fusion events in FL cells resulted in significant mixing between the first and second pulses of Tfn and their colocalization in endosomal compartments both at the periphery and in perinuclear regions of the cell (Fig 1A, see arrows). In contrast, in mutant cells (Fig 1A, bottom panel) there was very little mixing between the two pulses of Tfn, with the second pulse of Tfn^{AF568} remaining largely at the cell periphery, suggesting a delay in homotypic fusion and defects in nascent endocytic vesicle maturation and trafficking.

As early endosomes mature, their lumenal content becomes increasingly acidic through the action of V-ATPases (Forgac, 2007). To measure the rate and extent of acidification of Tfn-containing nascent endosomes, we incubated FL and ΔαAD cells with Tfn conjugated to the pH-sensitive probe pHrodo Red and followed the increase in fluorescence emission as an indicator of increased acidification of Tfn in early endosomes. In both cell lines, the fluorescence of internalized pHrodo Red-Tfn increased, indicating acidification, and reached a plateau within 5 min before slowly decreasing as Tfn moved into a less acidic recycling compartment (Fig 1B). However, the degree of acidification was significantly lower in mutant as compared to control cells, again indicating that early endosomal maturation is defective in these cells.

Homotypic and heterotypic fusion events during early endosome maturation aid the formation of sorting endosomes, from which Tfn recycles back to the cell surface via perinuclear recycling endosomes. Thus, we expected to see a defect in the rate of Tfn recycling, which we next determined by loading cells with a pulse of biotinylated-Tfn (BSS-Tfn) for different time points, followed by the recycling of BSS-Tfn back to the plasma membrane. Surprisingly, we observed that a significant portion of internalized BSS-Tfn preloaded with short pulses ($\leq$ 20 min) recycled with faster kinetics in ΔαAD cells (Fig 1C and Supplementary Fig S2A and B). Thus, a large fraction of nascent endocytic vesicles formed during dysregulated CME fail to mature and instead rapidly return to the plasma membrane. When perinuclear recycling endosomes were loaded with a longer pulse of BSS-Tfn (60 min), the rates of recycling were indistinguishable, indicating that these later stages of endocytic trafficking were unaffected (Supplementary Fig S2C).

During maturation, early endosomes sequentially acquire the Rab5 effectors APPL1 and EEA1 that function as scaffolding molecules on endosomal surfaces (Rink *et al*, 2005). Immunofluorescence of EEA1- (Fig 1D, Supplementary Fig S3A) and APPL1-positive (Fig 1D, Supplementary Fig S3B) early endosomes revealed their substantial accumulation in ΔαAD when compared to FL cells.

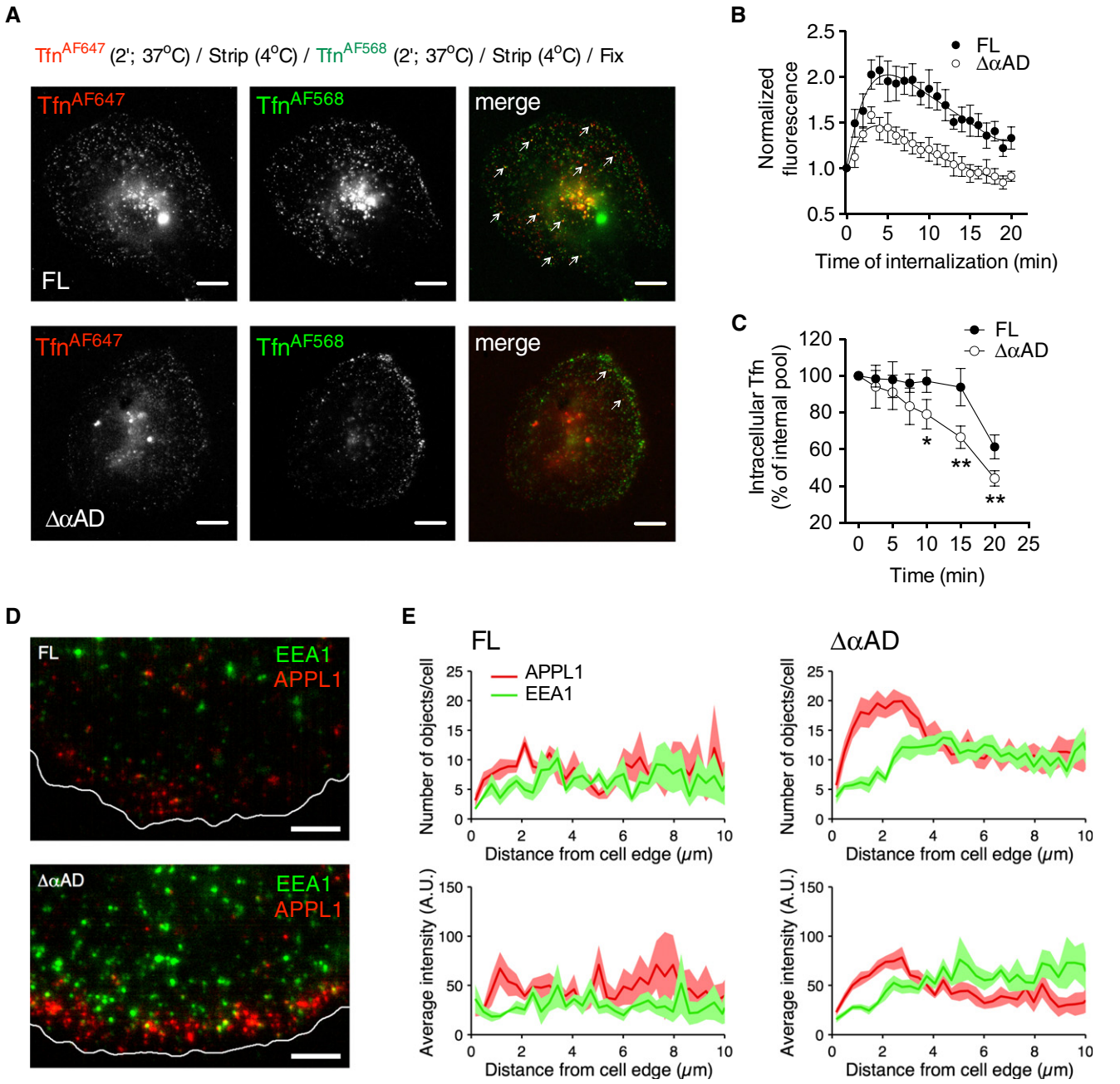

Figure 1. Dysregulated CME leads to aberrant trafficking of nascent CCVs.

A Fluorescence images of FL and ΔαAD cells after sequential 2-min pulses of Tfn^{AF647} (red), followed by Tfn^{AF568} (green); arrows indicate colocalization between Tfn^{AF647} and Tfn^{AF568}. Scale bars, 10 μm.

B Time-lapse normalized fluorescence showing the acidification profile of internalized pHrodo Red-Tfn in FL and ΔαAD cells. Data represent mean ± S.D., $n = 3$.

C Time course of BSS-Tfn recycling after internalization for a 5-min pulse. Percentage of Tfn recycling was calculated relative to the initial total internal pool of internalized ligand. Data represent mean ± S.D., $n = 3$. Two-tailed Student's t-tests were used to assess statistical significance. *$P < 0.05$, **$P < 0.005$.

D Peripherally localized APPL1- (red) and EEA1-positive (green) endosomes in FL and ΔαAD cells imaged by TIRFM at ~250 nm depth of the evanescent field. Scale bars, 5 μm.

E Quantification of the localization and intensities of APPL1 and EEA1 early endosomes in FL and ΔαAD relative to the cell edge (15 cells). The shaded areas indicate the confidence at a particular point, showing the different distributions in both FL and ΔαAD cells. Number of objects as function of distance: P-value < 5e-04 (permutation test).

Furthermore, APPL1- and EEA1-positive early endosomes displayed a significantly more peripheral localization in ΔαAD cells (Fig 1E). Given that there was no corresponding increase in the protein levels of either APPL1 or EEA1 (data not shown), we interpret the accumulation and localization of these intermediates as a delay in maturation. Together, these data establish that nascent endocytic vesicles

formed in ΔαAD cells have profound defects in subsequent vesicular trafficking and maturation.

Dysregulated CME alters cell signaling

CME plays an important role in the regulation of multiple signaling pathways (Le Roy & Wrana, 2005; Traub, 2009). Besides dysregulated CME and aberrant trafficking of nascent CCVs, the ΔαAD cells also exhibited enhanced cell proliferation (Fig 2A). The kinase Akt is known to orchestrate diverse fundamental processes, including cell proliferation. Consistent with this, we detected a significant increase in the steady-state activation/phosphorylation of Akt in ΔαAD cells (Fig 2B). The scaffold protein APPL1 has been shown to play an important role in the regulation of Akt (Schenck *et al*, 2008). Therefore, we next investigated whether the accumulation of APPL1-positive early endosomes contributed to the enhanced Akt activity measured in these cells. The siRNA-mediated knockdown of APPL1 in ΔαAD cells significantly reduced Akt phosphorylation, back to the levels seen in FL cells (Fig 2C and D).

Given the role of CME in regulating signaling, we next examined the effects of dysregulated CME on downstream signaling from activated EGF receptors. Stimulation of serum-starved cells with 20 ng/ml of EGF induced Akt activation (pT308 and pS473) to a much greater extent in ΔαAD cells compared to control cells (Fig 3A, quantification in B). We also observed increased ERK activation in response to EGF (Supplementary Fig S4A and B), but no significant increase under steady-state conditions (data not shown). Akt can activate multiple downstream pathways depending, in part, on its cellular localization (Palfy *et al*, 2012). The APPL1-dependent recruitment of Akt to early endosomes has been shown to regulate phosphorylation of GSK3β kinase but not TSC2, which is activated in the cytosol by Akt upon growth factor stimulation (Schenck *et al*, 2008) (Fig 3C). We therefore tested for differences in growth factor stimulation of these two proteins. Consistent with enhanced signaling from accumulated APPL1-positive endosomes, EGF-stimulated phosphorylation of GSK3β but not TSC2 was strongly enhanced in ΔαAD cells, relative to FL cells (Fig 3D and E). Taken together, these results indicate that dysregulated CME leads to the accumulation of early endosome intermediates that prolong and enhance specific downstream signaling pathways.

Dynamin-1 is specifically enlisted for rapid, compensatory endocytosis

The GTPase dynamin, which assembles into a fission apparatus at the necks of mature, deeply invaginated CCPs, is also recruited at early stages of CCP maturation (Damke *et al*, 1994; Ehrlich *et al*, 2004; Taylor *et al*, 2012) and has been proposed to function as a

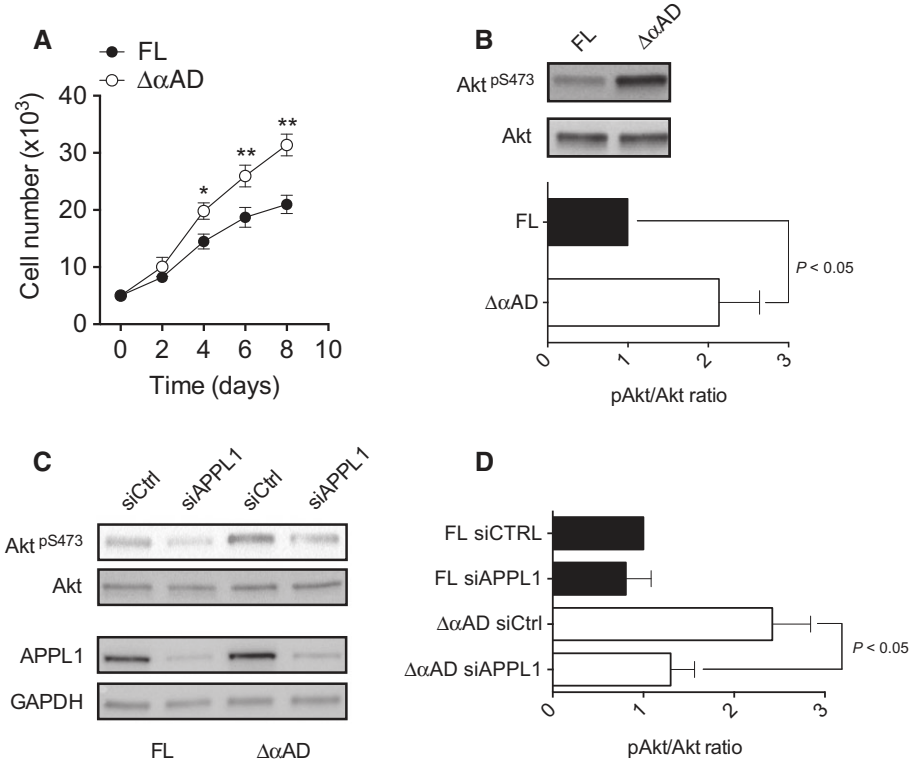

Figure 2. Enhanced proliferation and activation of Akt is regulated by the accumulation of APPL1-positive early endosomes.

A Increased proliferation rate in ΔαAD compared to FL cells (mean ± S.D., $n = 3$). Two-tailed Student's *t*-tests were used to assess statistical significance. $^{*}P < 0.05$, $^{**}P < 0.005$.

B Immunoblots of total and activated Akt (pS473) in FL and ΔαAD cells and quantification of pAkt/Akt intensity ratio (mean ± S.D., $n = 3$).

C RNAi-mediated knockdown of APPL1 and its impact on Akt activation (pAkt/Akt) in FL and ΔαAD cells.

D Quantification of pAkt/Akt intensity ratios in FL and ΔαAD cells treated with control and APPL1-siRNA (mean ± S.D., $n = 3$).

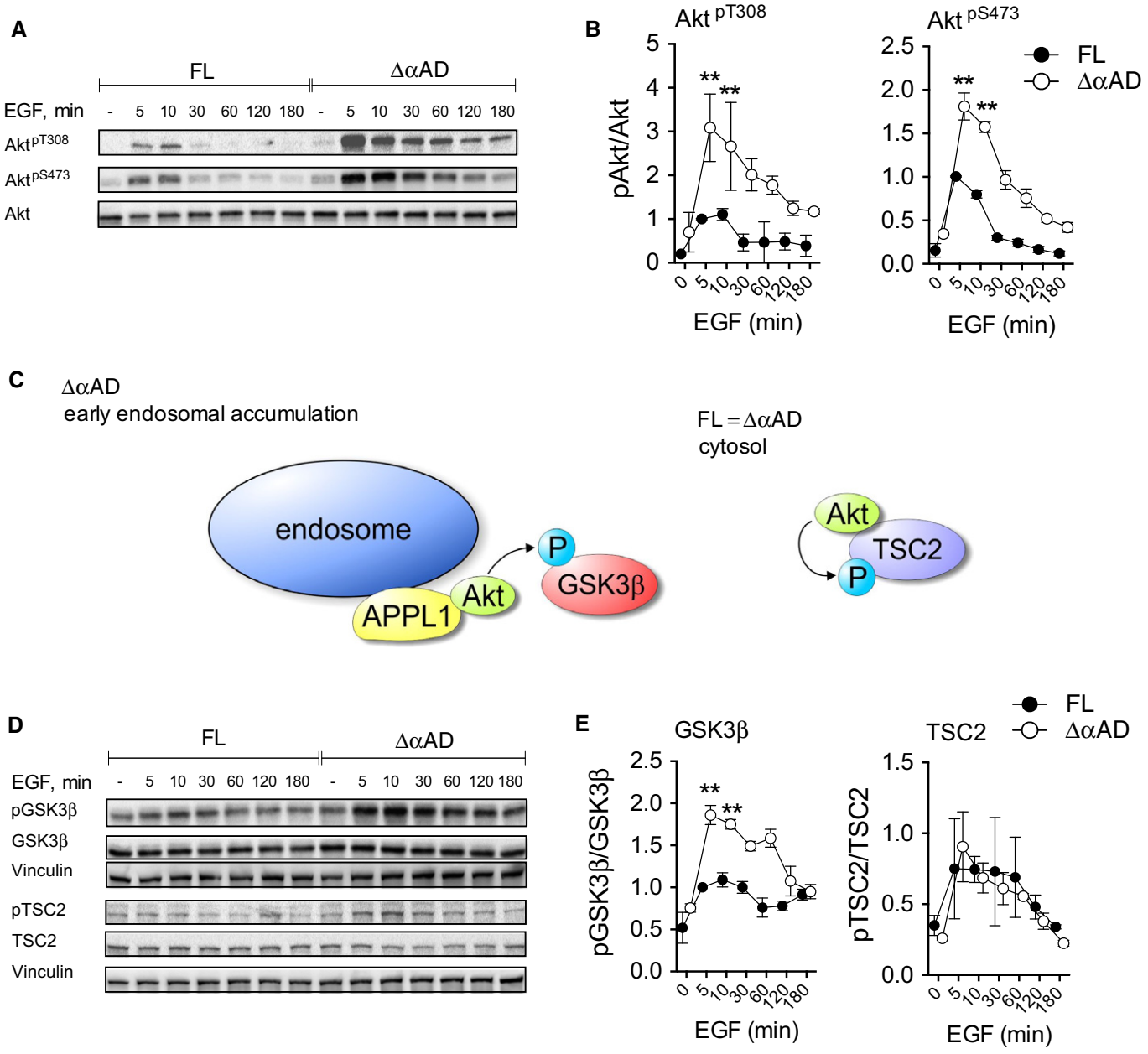

Figure 3. Dysregulated CME alters cell signaling.

A EGF stimulation profile (20 ng/ml; 0–180 min) of Akt (pS473 and pT308).

B Quantification of pAkt/Akt (pT308 and pS473) intensity ratios in FL and ΔαAD cells.

C Akt-enhanced phosphorylation/inactivation of GSK3β is mediated by APPL1 early endosomal accumulation in ΔαAD cells, whereas a cytosolic complex mediates TSC2 phosphorylation.

D GSK3β and TSC2 phosphorylation profiles upon EGF stimulation.

E Quantification of pGSK3β/GSK3β and pTSC2/TSC2 intensity ratios.

Data information: In (B, E), data represent mean ± S.D., $n = 3$. Two-tailed Student's t-tests were used to assess statistical significance. $^{**}P < 0.005$.

regulator of early, rate-limiting steps in CCV formation (Mettlen *et al*, 2009a; Aguet *et al*, 2013). Although Dyn1 is highly expressed in neuronal tissues and enriched at the synapse, transcriptional analyses reveal that mRNA levels for the Dyn1 and Dyn2 isoforms are similar in most tissues (dynamin-1: http://biogps.org/gene/1759/; dynamin-2: http://biogps.org/gene/1785/). Consistent with this, Dyn1 expression has been detected by Western blotting in many non-neuronal cell lines, including the RPE cells used here (Supplementary Fig S5A and B). Given their potential isoform-specific differences (Liu *et al*, 2011, 2012), we next investigated the effects of Dyn1 and Dyn2 siRNA-mediated knockdown on CME in control and ΔαAD cells.

As expected, the siRNA-mediated knockdown of Dyn2 potently inhibited CME in both FL and ΔαAD cells (Fig 4A and B). Strikingly,

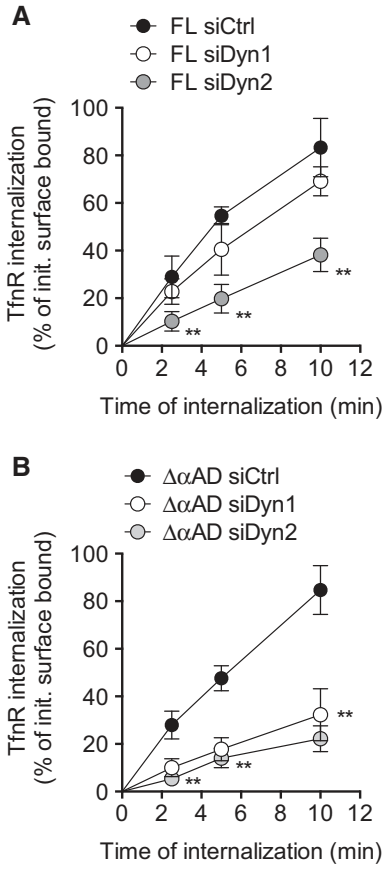

Figure 4. Dynamin-1 is specifically enlisted for rapid, compensatory endocytosis in ΔαAD cells.

A, B TfnR uptake measured in control-, Dyn1- and Dyn2-siRNA-treated FL (A) or ΔαAD cells (B). Percentage of TfnR uptake was calculated relative to the initial total surface-bound ligand at 4°C. Data represent mean ± S.D., $n = 3$. Two-tailed Student's *t*-tests were used to assess statistical significance. $^{**}P < 0.005$.

the siRNA-mediated knockdown of Dyn1 potently inhibited TfnR uptake in ΔαAD (Fig 4B), but had no significant effect on CME in FL cells (Fig 4A). Importantly, we did not detect differences in Dyn1 or Dyn2 expression levels between FL and ΔαAD cells, nor were there compensatory changes in expression upon knockdown of either Dyn1 or Dyn2 (Supplementary Fig S5). From these data, we conclude that Dyn1 is expressed but normally quiescent in these non-neuronal cells and can be activated to mediate rapid compensatory CME.

GSK3β directly regulates dynamin-1-dependent CME

We next investigated the mechanism by which Dyn1 is activated. At the synapse, Dyn1 activity is highly regulated by cycles of phosphorylation/dephosphorylation. For example, GSK3β-mediated phosphorylation of Ser774, which is not conserved in Dyn2, regulates Dyn1 activity (Clayton *et al*, 2010; Smillie & Cousin, 2011). Intriguingly, Akt is known to phosphorylate GSK3β and inhibit its activity (Schenck *et al*, 2008; Palfy *et al*, 2012), which might then allow for the consequent activation of Dyn1. Given that phosphorylation of both Akt and GSK3β is enhanced in ΔαAD cells (Figs 2 and 3), we wondered whether this signal transduction cascade could be responsible for activation of Dyn1 and induction of more rapid, compensatory CME. We first used a Ser774 phospho-specific antibody and confirmed that Dyn1 is phosphorylated in FL cells and that the steady-state levels of Dyn1 (pSer774) were indeed significantly decreased in ΔαAD cells (Fig 5A).

We then directly tested the role of this signaling cascade in the differential regulation of CME in FL and ΔαAD cells using several inhibitors of either Akt or GSK3β (Fig 5B). Uptake assays performed in the presence of the GSK3β inhibitors Bio (Supplementary Fig S6A and B) or CHIR-99021 (Supplementary Fig S6C) led to an increase in the rate of CME in control cells, while having no effect on ΔαAD cells (Fig 5C and D). This effect was due to activation of Dyn1, as it was abrogated by siRNA-mediated knockdown of Dyn1, but still evident upon knockdown of Dyn2 (Fig 5C). Correspondingly, treatment with the PI3K/Akt inhibitor LY294002 (Supplementary Fig S6A and B) or the more specific Akt inhibitor X (Supplementary Fig S6C) showed no effect on CME in FL cells, but reduced the rate of CME in ΔαAD cells to that seen upon siRNA-mediated knockdown of Dyn1 (Fig 5F).

Given the altered distribution of APPL1 endosomes seen in ΔαAD cells and their impact on Akt activation, we next examined the effect of APPL1 depletion on CME rates. As expected, and similar to the effect of Akt inhibition, the siRNA-mediated knockdown of APPL1 resulted in a significant decrease in the rate of CME in these cells, but not in control (FL) cells (Fig 6A). The generation of peripheral APPL1 early endosomes has been shown to be partially dependent on CME (Zoncu *et al*, 2009). Consistent with this and our biochemical studies, inhibition of Akt in ΔαAD cells led to a reduction in the amount of peripheral APPL1 early endosomes (Fig 6B). In contrast, in control cells the inhibition of GSK3β, which in turn activates Dyn1 and triggers dysregulated CME, leads to the accumulation of APPL1 early endocytic intermediates (Fig 6C).

To exclude the possibility that these effects are specific to ΔαAD mutant cells, we next asked whether Dyn1 could be activated via this signaling pathway in the parental ARPE-19 cells. As seen in FL cells, CME in untreated ARPE-19 cells was strongly dependent on Dyn2 but not Dyn1, and it was insensitive to Akt inhibitors (Fig 7A). Strikingly, the inhibition of GSK3β in ARPE-19 cells resulted in an increased rate of TfnR uptake, which was abrogated upon siRNA knockdown of Dyn1, but not Dyn2 (Fig 7B). Taken together, these results establish that Dyn1 can be directly activated through an Akt/GSK3β kinase cascade to increase the rate of CME.

The crosstalk between signaling and dynamins alters CCP dynamics and dysregulates CME

We previously showed that CCPs undergo a complex, multistep maturation process that is reflected in their broad lifetime distribution (Loerke *et al*, 2009; Aguet *et al*, 2013). We have also shown that CCPs that fail to recruit Dyn2 exhibit an exponentially decaying lifetime distribution, indicative of an unregulated process, and suggesting that dynamin might regulate early stages of CCP maturation (Loerke *et al*, 2009; Aguet *et al*, 2013). Finally, those few CCPs that are able to mature in ΔαAD cells also exhibit a near-exponential lifetime distribution reflective of an unregulated maturation process (Loerke *et al*, 2009; Aguet *et al*, 2013). Thus, we wondered whether the activation of Dyn1 might be sufficient to accelerate CCP maturation and alter its regulation. CCPs in ARPE-19 cells stably expressing EGFP-CLCa exhibit the expected broad lifetime distribution

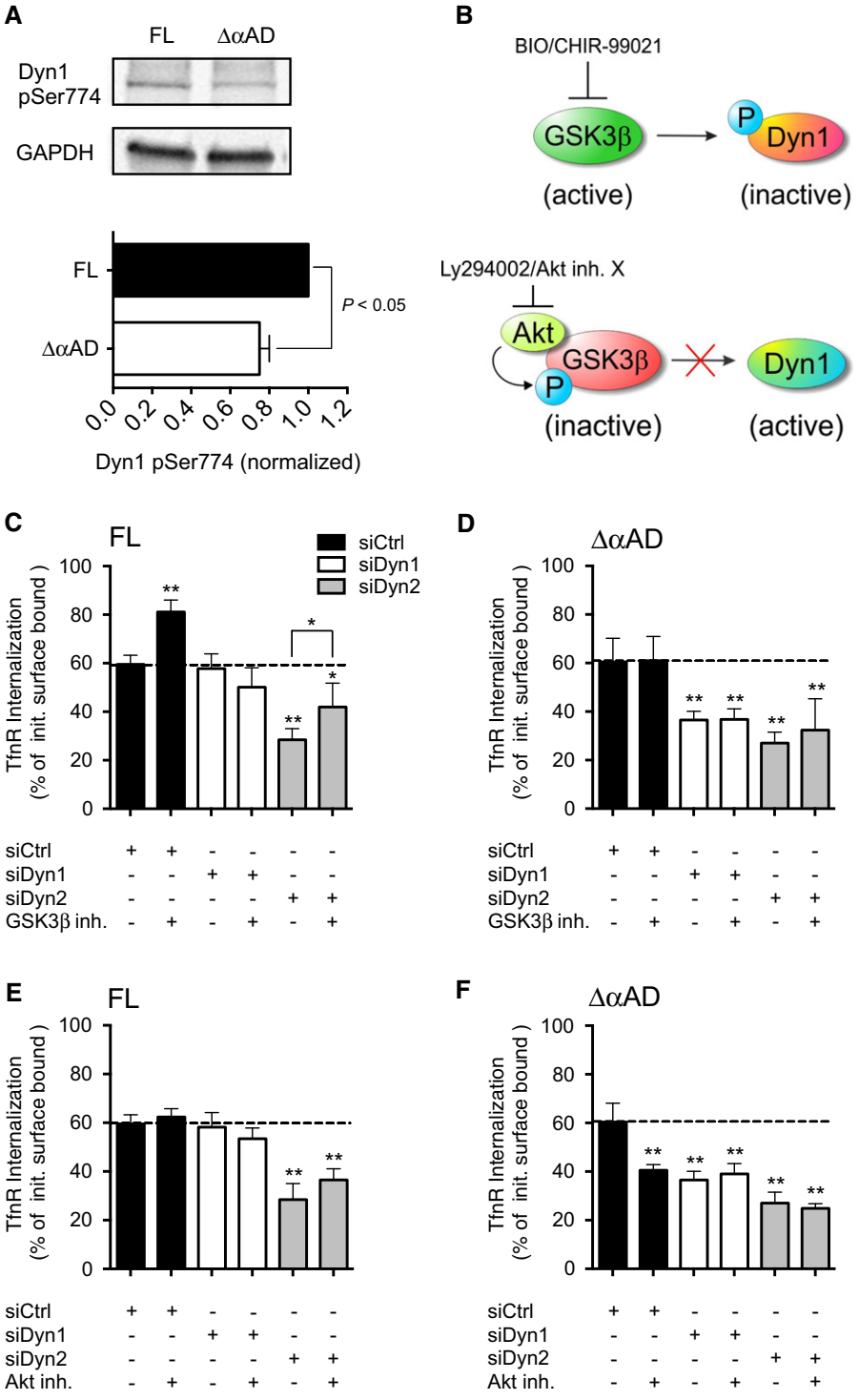

Figure 5. GSK3β directly regulates dynamin-1-dependent endocytosis in ARPE cells.

A Immunoblots and quantification of phosphorylated Dyn1 (pSer774) in FL and ΔαAD cells (mean ± S.D., $n = 3$). Two-tailed Student's t-tests were used to assess statistical significance.

B Potential differential impact of Akt/GSK3β signaling on Dyn1 activity in FL and ΔαAD cells.

C, D TfnR uptake (5-min pulse) measured in control-, Dyn1- and Dyn2-siRNA-treated FL (C) or ΔαAD cells (D), with or without the GSK3β inhibitor CHIR-99021 (10 μM).

E, F TfnR uptake (5-min pulse) measured in control-, Dyn1- and Dyn2-siRNA-treated FL (E) or ΔαAD cells (F), with or without the specific Akt inhibitor X (10 μM).

Data information: In (C–F), cells were pre-incubated with the corresponding inhibitors for 30 min prior to measuring internalization of Tfn. Percentage of TfnR uptake was calculated relative to the initial total surface-bound ligand at 4°C. Data represent mean ± S.D., $n = 3$. Two-tailed Student's t-tests were used to assess statistical significance. $^*P < 0.05$, $^{**}P < 0.005$.

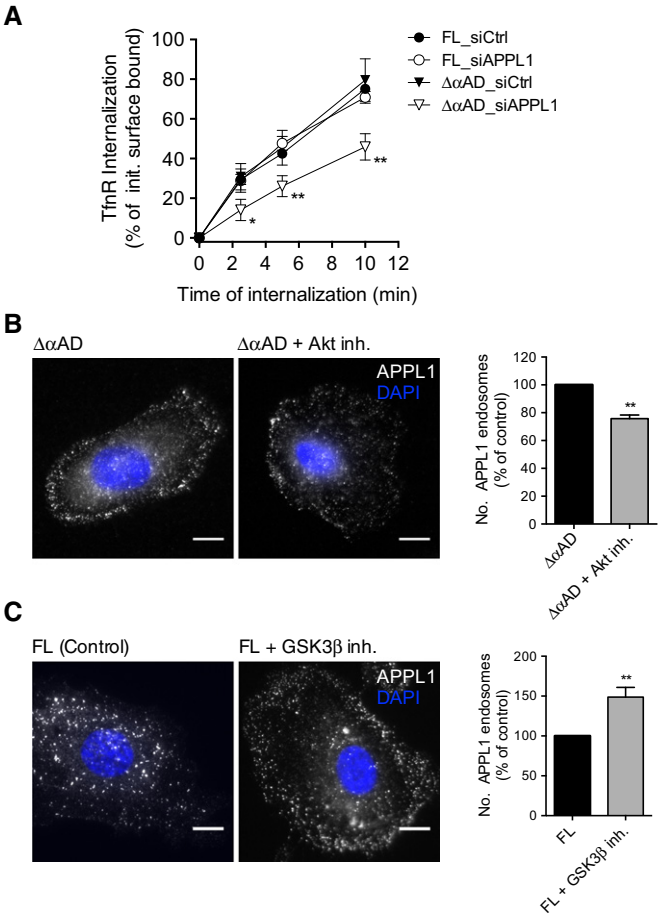

Figure 6. APPL1 regulates compensatory CME in ΔαAD cells.

A TfnR uptake measured in control- or APPL1-siRNA-treated FL and ΔαAD cells. Percentage of TfnR uptake was calculated relative to the initial total surface-bound ligand at 4°C. Data represent mean ± S.D., $n = 3$. Two-tailed Student's *t*-tests were used to assess statistical significance. $^{*}P < 0.05$, $^{**}P < 0.005$.

B Distribution and quantification of APPL1-containing early endosomes in ΔαAD cells after inhibition with the Akt inhibitor X (10 μM), as measured by immunofluorescence.

C Distribution and quantification of APPL1-containing early endosomes in FL cells after incubation with the GSK3β inhibitor CHIR-99021 (10 μM), as measured by immunofluorescence.

Data information: In (B, C), cells were pre-incubated with the corresponding inhibitors for 30 min. Data represent normalized number of endosomes (mean ± S.D.) counted in 15 cells/condition. Two-tailed Student's *t*-tests were used to assess statistical significance. $^{**}P < .005$. Scale bars, 10 μm.

(Fig 7C, red curve) reflective of a multi-step regulated maturation process. Strikingly, upon acute treatment with the GSK3β inhibitor CHIR-99021, the curve shifts to a quasi-exponentially decaying lifetime distribution, indicative of a less regulated process (Fig 7C, green curve). Moreover, the median lifetime of CCPs decreases from ~53 s in control cells to ~35 s in GSK3β-inhibited cells, in agreement with the more rapid Tfn uptake measured biochemically. Consistent with the biochemical studies shown in Figs 4 and 5, the siRNA-mediated knockdown of Dyn1 alone had no effect on CCP dynamics in ARPE-19 cells (Fig 7C, red and blue curves); however, Dyn1-depleted cells no longer responded to inhibition of GSK3β (Fig 7C, purple curve). From these data, we conclude that the effects of GSK3β inhibition on CME are through phosphorylation of Dyn1 and that its activation alters the rate and regulation of early stages in CCP maturation. Unexpectedly, we also detected a dramatic increase in the rate of CCP initiation upon inhibition of GSK3β, which was again completely dependent on Dyn1 (Fig 7D). These results indicate that signaling through Akt/GSK3β modulates the activity of Dyn1, leading to enhanced rates of CCP initiation and maturation, as well as altered regulation of CME in normal cells.

Akt signaling activates dynamin-1 in H1299 lung cancer cells

The Akt/GSK3β signaling pathway is highly activated in many cancers, and it has been suggested that CME can be dysregulated in cancer (Mosesson *et al*, 2008; Mellman & Yarden, 2013). Therefore, we next tested whether Dyn1 might function in CME in cancer cells displaying high levels of Akt phosphorylation, such as H1299, non-small cell lung cancer (NSCLC) adenocarcinoma cells (Hernandez *et al*, 2013). Indeed, we found by siRNA-mediated knockdown of Dyn1 and Dyn2 that H1299 cells are partially dependent on Dyn1 for efficient TfnR uptake (Fig 8A), while also relying on Dyn2. Consistent with activated Dyn1 in H1299 cells, CME is only slightly accelerated in the presence of GSK3β inhibitors, but markedly reduced by inhibition of Akt (Fig 8B). To further explore Dyn1 function in cancer cells, we generated a Dyn1 knockout (KO) H1299 cell line using CRISPR-Cas9n and then reconstituted these cells with either WT-Dyn1-EGFP or S774A-Dyn1-EGFP, a mutant that cannot be phosphorylated by GSK3β (Fig 8C). Consistent with the effects of Dyn1 siRNA treatment of H1299 cells, knockout of Dyn1 in H1299 (Fig 8D, white bars) resulted in an ~40% decrease in the rate of TfnR uptake, to approximately the same level as inhibition of Akt in parent cells (Fig 8D, black bars). Importantly, Akt inhibition did not further reduce TfnR uptake in Dyn1 KO cells (Fig 8D, white bars), suggesting that the effects of Akt inhibition on CME are indeed dependent on Dyn1. Reconstitution of Dyn1 KO H1299 cells with either WT-Dyn1-EGFP (Fig 8D, light gray bars) or S774A-Dyn1-EGFP (Fig 8D, dark gray bars) fully restored the rate of TfnR uptake back to control levels, indicating that Dyn1-EGFP is fully active in these cells. That expression of S774A-Dyn1-EGFP did not increase the rate of CME suggests that other phosphorylation sites, for example S778, which are required for GSK3β recognition (Clayton *et al*, 2010) might also regulate dynamin-1 activity. Importantly, whereas WT-Dyn1-EGFP-expressing cells still showed sensitivity to Akt inhibition, S774A-Dyn1-EGFP-expressing cells were no longer responsive to Akt inhibition. These results establish that the effects of Akt inhibition on CME are primarily mediated by Dyn1 activation through phosphorylation of S774 and that enhanced Akt signaling in cancer cells can indeed lead to activation of Dyn1 and dysregulated CME.

Discussion

The findings presented here provide direct evidence for the role of dynamins as key regulators of early steps of CCP formation and demonstrate that alterations in the regulation of CME can profoundly influence downstream endosomal maturation and trafficking. We establish the existence of an Akt/GSK3β-dependent

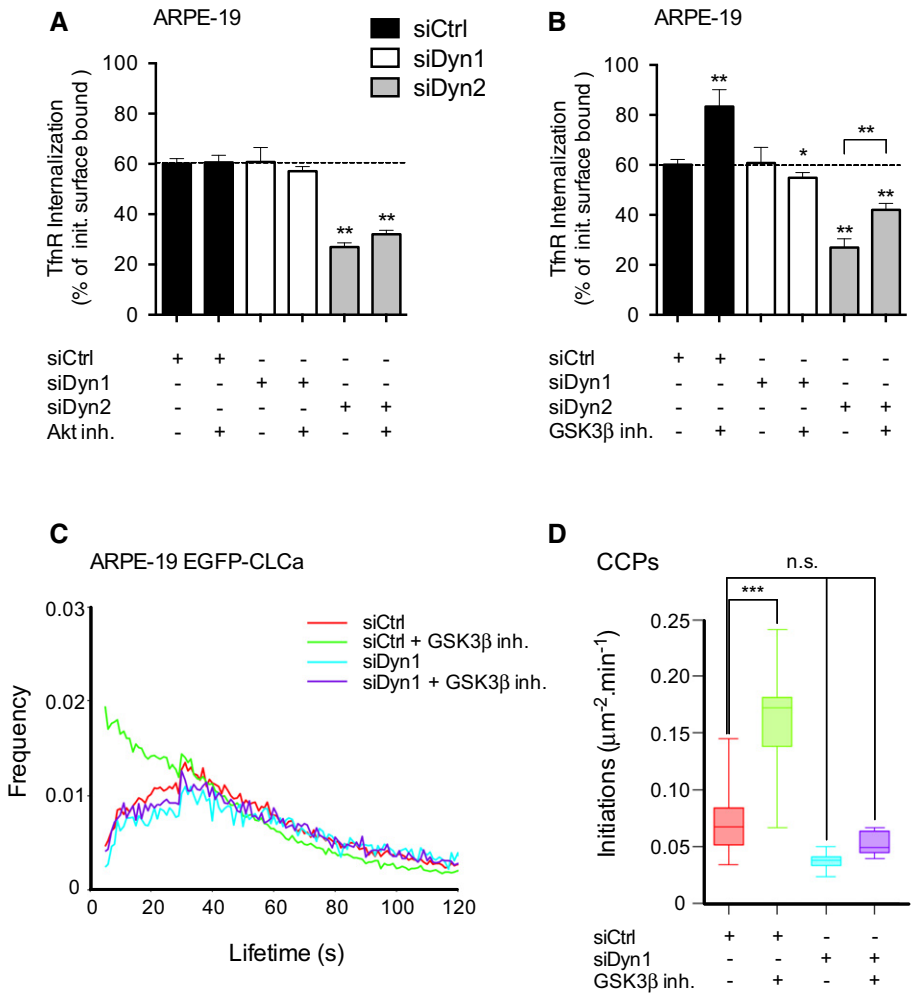

Figure 7. Crosstalk between signaling and dynamin-1 alters CCP dynamics and CME efficiency.

A, B GSK3β regulates dynamin-1-mediated CME in WT ARPE cells. TfnR uptake (5-min pulse) measured in control-, Dyn1- and Dyn2-siRNA-treated ARPE WT cells with or without pre-incubation with the Akt inhibitor X (10 μM) (A). Effects of GSK3β inhibition (CHIR-99021, 10 μM) on TfnR uptake in ARPE-19 WT cells treated with control, Dyn1- and Dyn2-siRNA (B). Cells were pre-incubated with the inhibitors for 30 min prior to measuring internalization of Tfn. Percentage of TfnR uptake was calculated relative to the initial total surface-bound ligand at 4°C. Data represent mean ± S.D., $n = 3$. Two-tailed Student's *t*-tests were used to assess statistical significance. $^{*}P < 0.05$, $^{**}P < 0.005$.

C Average lifetime distributions of *bona fide* CCPs in FL cells treated with control siRNA, the GSK3β inhibitor CHIR-99021 (10 μM) and Dyn1-siRNA alone or in combination with the GSK3β inhibitor, as indicated.

D Initiation density of all detected *bona fide* CCPs with lifetime > 5 s, for the conditions indicated. Box plots show median, 25th and 75th percentiles, and outermost data points. Data were obtained from 15 cells/condition. $^{***}P < 10^{-10}$, permutation test.

signaling cascade in non-neuronal cells that directly links activation of dynamin-1 to alterations in the early stages in CCP initiation and maturation. Together, these results suggest the intriguing possibility that signaling receptors could generate a feed-forward signal through Akt and GSK3β to activate dynamin-1, dysregulate CME and enhance signaling properties.

Live cell imaging and quantitative image analysis of CME had revealed the existence of a subpopulation of short-lived, abortive CCPs (Ehrlich *et al*, 2004; Loerke *et al*, 2009; Taylor *et al*, 2012; Aguet *et al*, 2013). Our previous studies reporting that the proportion of abortive vs. productive CCPs is dependent on cargo loading (Loerke *et al*, 2009; Liu *et al*, 2010) and affected by siRNA knockdown of a subset of EAPs (Mettlen *et al*, 2009b) led us to propose the existence of an endocytic checkpoint gating CCP maturation. In further support of this model, here we show that the products of CME (i.e., nascent endocytic vesicles) formed in ΔαAD cells by bypassing this regulation are functionally altered: Homotypic fusion and subsequent early endosomal maturation stages are significantly delayed, endosome acidification is reduced, and the portion of TfnRs undergoing rapid recycling is increased. Together, these data further support the existence and significance of an endocytic checkpoint that monitors the fidelity of CME. Not addressed here, and in need of further study, are the molecular mechanisms involved in sensing defects in CCP formation and in actively turning over aberrant CCPs. It will also be important to identify the precise molecular alterations in nascent CCVs that underlie the dramatic changes seen in their downstream maturation. Identification of these differences would provide important insight into what aspects of CCP maturation

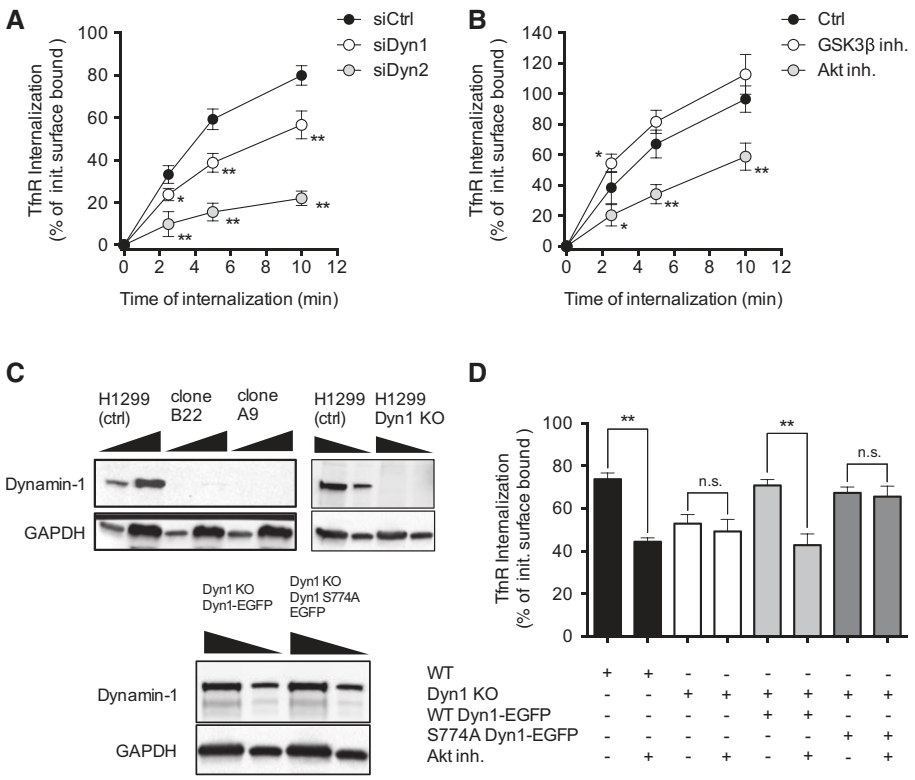

Figure 8. Dynamin-1 activation in H1299 (NSCLC) cells.

A TfnR uptake measured in control-, Dyn1- and Dyn2-siRNA-treated H1299 cells.

B Effects of Akt inhibition (Akt inhibitor X, 10 μM) and GSK3β inhibition (CHIR-99021, 10 μM) on TfnR uptake in H1299 cells.

C Analysis of two representative single clones (B22, A9) and characterization of Dyn1 KO cell line chosen for further assays. Analysis of Dyn1 expression in Dyn1 KO cells reconstituted with Dyn1-EGFP WT or Dyn1 S774A-EGFP, as assessed by Western blotting (two different concentrations: 60 and 20 μg of protein loaded on the gel).

D TfnR uptake (5-min pulse) measured in control, Dyn1-KO, Dyn1-KO reconstituted with Dyn1-WT or Dyn1-S774A cells, with or without pre-incubation with the Akt inhibitor X (10 μM).

Data information: Cells were pre-incubated with the inhibitors for 30 min prior to measuring internalization. Percentages of TfnR uptake were calculated relative to the initial total surface-bound ligand at 4°C. Data represent mean ± S.D., $n = 3$. Two-tailed Student's *t*-tests were used to assess statistical significance. *$P < 0.05$, **$P < 0.005$.

are monitored by the endocytic checkpoint. While beyond the scope of this study, candidates include defects in the packaging of SNARE proteins or the V-ATPase, both of which might be required for subsequent targeting and fusion events.

Here we have focused on identifying the compensatory mechanism by which CME is fully restored in mutant cells despite a severe defect in early stages of CCP maturation. We show that the accumulation of APPL-1 endosomes leads to the constitutive activation of Akt and phosphorylation of GSK3β to suppress its inhibitory phosphorylation of endogenous Dyn1. Activation of Dyn1 drives rapid, compensatory endocytosis in these non-neuronal cells. Most studies have focused on the burst of dynamin recruitment to promote membrane fission at the end of CCP maturation (Doyon *et al*, 2011; McMahon & Boucrot, 2011; Ferguson & De Camilli, 2012); however, there exists growing evidence that dynamin also functions in controlling early, rate-limiting stages of CCP maturation (Sever *et al*, 1999, 2000; Loerke *et al*, 2009; Taylor *et al*, 2012; Aguet *et al*, 2013). The data presented here strongly supports that dynamins can function, in an isoform-specific manner, as master regulators of CME.

Although Dyn1 is highly expressed in neurons and is generally considered to be a neuron-specific isoform, mRNA levels of Dyn1 and Dyn2 are actually comparable in most tissues. Consistent with this, the signaling pathway we have identified is also operable in parental ARPE-19 cells and other non-neuronal cells. Acute inhibition of GSK3β accelerates CME in a Dyn1-dependent, but Dyn2-independent manner. Strikingly, CCP dynamics in ARPE-19 cells acutely treated with GSK3β inhibitors fully mirror those of productive, curved CCPs in ΔαAD cells. Specifically, the rate of CCP initiation approximately doubles and productive CCPs mature in a more rapid and unregulated manner (compare Fig 6A and B this report with Figs 6E and 7E in Aguet *et al*, 2013). Thus, we conclude that Dyn1 alters the regulation of early stages of CME including CCP initiation and maturation. A role for Dyn1 in CCP assembly has also been suggested by a recent study in which acute photoablation of Dyn1 in Drosophila prevented AP2 and clathrin assembly at the synapse (Kasprowicz *et al*, 2014).

We previously showed that Dyn1 and Dyn2 have distinct biochemical properties (Liu *et al*, 2011) that correlate with their differential effects on CME. Dyn1 is a powerful curvature generator

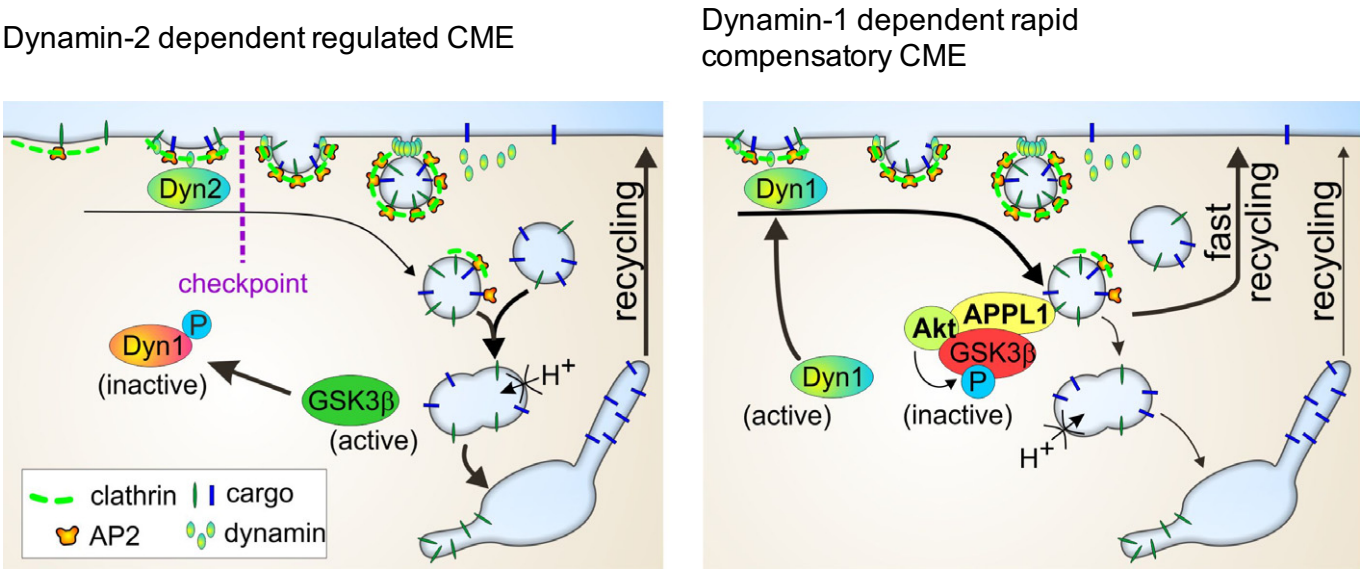

Figure 9. Differential functions for dynamin-1 and dynamin-2 in the regulation of CME.
Left: We propose that Dyn2, which is recruited early to CCPs (Aguet *et al*, 2013; Cocucci *et al*, 2014), regulates CME as part of a proposed endocytic checkpoint. Right: Activation of Dyn1, through an APPL1-endosome-dependent Akt/GSK3β signaling cascade, increases the rate of CCP initiation and triggers rapid, dysregulated CME that bypasses a fidelity-monitoring step. Consequently, the nascent endocytic vesicles formed are defective in downstream trafficking: Homotypic fusion events and the maturation of APPL1- and EEA1-positive endosome are delayed, TfnR rapidly recycles back to the cell surface, and endosomal acidification is reduced. Our findings establish that dynamin isoforms differentially regulate early stages of CME.

that could compensate, in part, for the defect in curvature generation of nascent CCPs in ΔαAD cells. In contrast, Dyn2 is highly curvature sensitive, yet is targeted more efficiently to CCPs by virtue of its divergent Pro/Arg-rich domain (Liu *et al*, 2011). While associated with CCPs, Dyn2 could monitor early stages of maturation. Formation of a narrow neck at the base of fully mature and deeply invaginated CCPs could trigger Dyn2 assembly and fission. Evolutionary history also supports a regulatory role for dynamin (Liu *et al*, 2012) in that it appears much later in evolution than the core CME machinery, which dates back to the earliest common eukaryotic ancestor (Field *et al*, 2007). Further work will be needed to understand the isoform-specific differences behind Dyn1 and Dyn2 regulation of CME and to identify specific up- and downstream effectors of this complex multi-step process. We note that CME in ΔαAD cells depends on both Dyn1 and Dyn2. Whether they work together at single CCPs or independently at subsets of CCPs remains to be determined.

Although endocytosis and cellular signaling have been previously viewed as separate processes, endocytosis is now recognizably linked to many aspects of cellular signaling (Sorkin & von Zastrow, 2009; Di Fiore & von Zastrow, 2014). Recently, stimulation of cells with EGF has been shown to modulate the number of early endosomes (Villasenor *et al*, 2015), in a mechanism that can in turn potentially regulate signaling. Moreover, a recently generated map of endocytic membrane trafficking revealed new potential links between signaling and endocytic pathways (Liberali *et al*, 2014). Strikingly, whereas Akt2 inhibition/knockdown severely reduced Tfn uptake, inhibition of GSK3β strongly enhanced CME in HeLa cells (Liberali *et al*, 2014). These results independently confirm our findings, support the importance of the Akt/GSK3β axis in regulating CME and further suggest that our results are likely valid in other cell types. Here we establish that this kinase cascade operates through the activation of Dyn1 leading to rapid and dysregulated endocytosis (Fig 9). Whether Dyn1 can be activated in a cargo-selective manner to alter the dynamic behavior and trafficking of a specific subset of CCPs and CCVs is an intriguing possibility worthy of further study.

The crosstalk between aberrant signaling and the regulation of dynamins, which we have shown can lead to enhanced proliferation, may partially explain the impact of dysregulated CME in several diseases, including cancer. Given that Akt is overactive in numerous tumor cells, the activation of this signaling cascade could in turn induce significant differences in the dynamics of CME, lead to the accumulation of early endosomal intermediates and rapid receptor recycling and thus serve as a potent generator of survival signals that sustain high proliferative activity. In this way, activating Dyn1 might function as a feed-forward mechanism to enhance proliferative signals. Indeed, our analysis of the roles of Dyn1 and Akt in regulating CME in H1299 NSCLC cells supports this view. Interestingly, Dyn1 was found to be overexpressed in certain cancers, including leukemia, lung and colon adenocarcinomas (Haferlach *et al*, 2010; Hong *et al*, 2010); hence, the overexpression and/or potential Akt-driven activation of Dyn1 may have profound implications for the role of dysregulated CME in cancer.

Materials and Methods

Cell culture

ARPE-19 cells reconstituted with full-length (FL) or ΔAD α-adaptin were derived as previously described (Aguet *et al*, 2013). cDNA

encoding the full-length (FL) or truncated ΔAD α-adaptin was kindly provided by M.S. Robinson (Cambridge Institute for Medical Research). Expression of α-adaptins within each stable cell cohort was determined by Western blotting using the anti-AP2α (#AC1-M11, Pierce); the cohort with the expression level closest to endogenous α-adaptin was chosen for further experiments. All cell lines were grown under 5% CO_2 at 37°C in DMEM high glucose medium (Life Technologies) supplemented with 20 mM HEPES, 10 mg/ml streptomycin, 66 μg/ml penicillin and 10% (v/v) fetal calf serum (FCS, HyClone).

Transferrin receptor internalization and recycling from endosomal compartments

Transferrin (Tfn) internalization and recycling experiments were performed using anti-TfnR mAb (HTR-D65) (Schmid & Smythe, 1991) or biotinylated-Tfn (BSS-Tfn), respectively. ARPE-19 cells were grown overnight in 96-well plates at a density of 2.0×10^4 cells/well and pre-incubated with 4 μg/ml of D65 in Tfn assay buffer (PBS^{4+}: PBS supplemented with 1 mM $MgCl_2$, 1 mM $CaCl_2$, 5 mM glucose and 0.2% bovine serum albumin) at 4°C for 30 min. Cells were washed (3× PBS^{4+}) to remove unbound ligand and further incubated in the presence (continuous uptake) of additional ligand at 37°C for the indicated time points. Cells were then immediately cooled down (4°C) to arrest internalization. Following a washing step to remove unbound ligand (3× PBS^{4+}), the remaining surface-bound ligand was removed from the cells by an acid wash step (5 × 2 min 0.2 M acetic acid, 0.2 M NaCl, pH 2.5). Cells were washed with PBS and then fixed in 4% paraformaldehyde (PFA) (Electron Microscopy Sciences) in PBS for 20 min and further permeabilized with 0.1% Triton X-100/PBS for 10 min. Internalized D65 ligand was assessed using a goat anti-mouse HRP-conjugated antibody (Life Technologies), further developed with OPD (P1536, Sigma-Aldrich), and the reaction was stopped by using 5 M H_2SO_4. The absorbance was read at 490 nm (Biotek Synergy H1 Hybrid Reader). Internalized ligand was expressed as the percentage of the total surface-bound ligand at 4°C (i.e., without acid wash step), measured in parallel.

For Tfn internalization in FL and ΔαAD cells using the GSK3β inhibitors Bio (Sigma) or CHIR-99021 (Sigma), and the PI3K/Akt inhibitor LY294002 (Calbiochem) or the Akt inhibitor X (Calbiochem), cells were initially pre-incubated in the absence (i.e., control) or presence of the indicated inhibitor (10 μM) for 30 min at 37°C, followed by pre-incubation with 4 μg/ml of D65 in Tfn assay buffer at 4°C for 30 min, in the continued absence or presence of the inhibitor. Tfn internalization assays were then performed as described above. Percentage of Tfn uptake was calculated relative to the initial total surface-bound ligand at 4°C for all the assays.

For the recycling of Tfn from endosomal compartments, cells were pulsed for different time points (5-60 min) with 8 μg/ml of BSS-Tfn at 37°C. Following internalization, plates containing cells were transferred to ice, washed with cold PBS and acid-washed to remove surface-bound ligand. Cells were then incubated in PBS^{4+} containing 2 mg/ml of unlabeled Tfn at 37°C for the indicated time points. Remaining BSS-Tfn that recycled to the surface was again removed by acid wash, and the cells were further processed as described for the internalization assay, but this time using streptavidin-POD (Roche). The decrease in intracellular Tfn (recycling) was calculated relative to the total internal pool of ligand internalized.

siRNA transfection

ARPE-19 cells were treated with a previously established siRNA sequence using RNAiMAX (Life Technologies, Carlsbad, CA, USA) to silence endogenous proteins, following the manufacturer's instructions. Briefly, 110 pmol of the indicated siRNA and 6.5 μl of RNAiMAX reagent were added in 2 ml of OptiMEM (Life Technologies) in each well of a 6-well plate containing cells for 4 h. Transfection was performed at day 1 and day 3 after plating, and experiments were performed at day 5. The exogenously expressed FL and ΔAD α-adaptins harbor mutations that confer resistance to siRNA silencing. siRNA oligos used to target the following proteins were endogenous α-adaptin (5′-GAGCAUGUGCACGCUGGCCA-3′), dynamin-1 (5′-GGCUUACAUGAACACCAACCACGAA-3′), dynamin-2 (Dyn2_1: 5′-CCGAAUCAAUCGCAUCUUCUU-3′ and Dyn2_2: 5′-GACAUGAUCCUGCAGUUCAUU-3′), as well as CHC as previously described (Huang *et al*, 2004). The AllStars Negative siRNA non-targeting sequence was purchased from Qiagen.

Microscopy/fluorescence-based assays

Immunofluorescence: ARPE-19 FL and ΔαAD cells (1.5×10^5 cells per well in a 6-well plate) grown O/N on glass cover slips were washed with PBS and fixed in 4% PFA in PBS for 20 min at room temperature, permeabilized with 0.1% Triton X-100 for 10 min and further blocked with Q-PBS (0.01% saponin, 2% BSA, 0.1% lysine, pH 7.4) for 30 min. After three washes with PBS, cells were incubated with a mouse anti-EEA1 antibody (#610457, BD Transduction Labs) or a rabbit anti-APPL1 (#3858, Cell Signaling) in Q-PBS for 1 h using the recommended dilution. Cells were further washed three times with PBS and further incubated with suitable AlexaFluor®-labeled secondary antibodies (Life Technologies) for 45 min. After three additional washes with PBS, samples were mounted on Fluoromount G (Electron Microscopy Sciences) on glass slides and examined using a 100 × 1.49 NA objective (Nikon) mounted on an epifluorescence Ti-Eclipse inverted microscope.

Tfn pulse/chase: Tfn^{AF568} and Tfn^{AF647} were obtained from Life Technologies. For dual-pulse experiments using fluorescent Tfn, FL and ΔαAD cells were initially pulsed with 4 μg/ml of Tfn^{AF647} for 2 min. Following a cold washing step to remove unbound ligand (3× PBS; 4°C), the remaining surface-bound ligand was removed by an acid wash step (3 × 2 min 0.2 M acetic acid, 0.2 M NaCl, pH 2.5). Cells were washed with PBS and then pulsed with 4 μg/ml of Tfn^{AF568} for 2 min, washed with cold PBS (4°C), acid-washed again and fixed in 4% paraformaldehyde (PFA) (Electron Microscopy Sciences) in PBS for 20 min. After three additional washes with PBS, samples were mounted on Fluoromount G (Electron Microscopy Sciences) on glass slides and examined using a 100 × 1.49 NA objective (Nikon) mounted on a Ti-Eclipse inverted microscope. EEA1- and APPL1-immunostained cells were imaged with an exposure time of 200 ms for both channels using a CoolSNAP HQ2 monochrome CCD camera with 6.45 × 6.45 μm^2 pixels (Photometrics, Tucson, AZ, USA).

Endosomal acidification: Time-lapse of Tfn internalization and acidification in FL and ΔαAD cells was performed by incubating cells with pHRodo-Tfn and recording the fluorescence emission (585 nm) every 60 s for 20 min using a Synergy H1 Hybrid Multi-Mode Microplate Reader.

EEA1 and APPL1 staining and analysis by TIRFM

Detection of fluorescence spot signals by TIRFM

Cells expressing EGFP-CLCa were immunostained for APPL1 (#3858, Cell Signaling) and EAA1 (#610457, BD Transduction Labs), followed by labeled secondary antibodies (Life Technologies). Fluorescent signals, illuminated using an incident angle set to visualize 250 nm from the coverslip, were detected using the spot detection algorithm as previously described (Aguet *et al*, 2013). Clathrin-coated structures and early endosomes were assumed to be diffraction-limited, producing a signal that is well approximated by a 2D Gaussian function in TIRF microscopy. Fluorescence signals were identified by numerically fitting a 2D Gaussian at candidate locations, and statistically testing the amplitude against the residual background noise estimated at each location. The detection was performed independently for the three fluorescence channels.

Identification of cell boundaries

Cell boundaries were automatically identified from the cytosolic background of EGFP-CLCa. The raw images were first smoothened using a Gaussian filter (S.D. = 5 pixels). The intensity distribution of the smoothened image was always bimodal, with the two modes representing background signal outside cells and fluorescence inside cells. A threshold was automatically selected as the local minimum between the two modes.

Object density relative to cell boundary

Object densities relative to the cell boundary were calculated from all objects that were closer to a cell boundary than the image border. The densities were normalized by the area of the band of pixels equidistant from the cell edge corresponding to each bin of the density histogram.

Western blotting

Cells were washed three times with PBS and harvested/resuspended in 100–150 μl of reducing Laemmli sample buffer. The cell lysate was boiled for 10 min and 30 μg of cell lysate was loaded onto an SDS gel. After transferring to a PVDF membrane, membranes were probed with antibodies against the following proteins: APPL1 (#3858, Cell Signaling), phospho-Akt S473 (#4060, Cell Signaling), phospho-Akt T308 (#13038, Cell Signaling), Akt (#9272, Cell Signaling), phospho-ERK (#4370, Cell Signaling), ERK (sc-93, Santa Cruz Biotechnology), phospho-TSC2 (#3611, Cell Signaling), TSC2 (sc-893, Santa Cruz Biotechnology), phospho-GSK3β (#5558, Cell Signaling), GSK3β (#610201, BD Transduction Laboratories), dynamin-1 (ab52852, Abcam), dynamin-1 phospho-S774 (ab55324, Abcam) and dynamin-2 (sc-6400, Santa Cruz Biotechnology), according to the manufacturers' instructions.

Cell proliferation and EGF-dependent signaling

ARPE-19 FL and ΔαAD cells (1.0×10^6 cells) were seeded in a 6-cm dish containing DMEM with 10% FBS. Eight hours after seeding, cells were washed three times with PBS and starved in DMEM containing 0.2% FBS for 16 h. One dish was left untreated (i.e., control). The remaining dishes were treated with 20 ng/ml of EGF for the indicated time points (0–180 min). At the end of each time point, cells were washed three times with PBS and harvested/resuspended in 100–150 μl of reducing Laemmli sample buffer. The cell lysate was boiled for 10 min, and 30 μg of cell lysate was subjected to SDS–PAGE. After transferring to a PVDF membrane, the membrane was used to probe with several EGF/EGFR downstream effectors as described above. Cell proliferation was assessed by MTS assay (Promega), according to the manufacturer's instructions.

TIRF microscopy

Total internal reflection fluorescence (TIRF) microscopy was performed as previously described (Loerke *et al*, 2009). Briefly, RPE cells expressing EGFP-CLCa were imaged using a 100 × 1.49 NA Apo TIRF objective (Nikon) mounted on a Ti-Eclipse inverted microscope equipped with the Perfect Focus System (Nikon). During imaging, cells were maintained in DMEM lacking phenol red and supplemented with 2.5% fetal calf serum. Time-lapse image sequences from different cells were acquired at a frame rate of 1 frame/s and exposure time of 150 ms using a CoolSNAP HQ2 monochrome CCD camera with 6.45 × 6.45 μm^2 pixels (Photometrics).

Image and data analysis

All image and data analyses were carried out in Matlab (MathWorks, Natick, MA, USA), using custom-written software. Up-to-date versions of the software will be made available at http://lccb.hms.harvard.edu/software.html.

Generation of dynamin-1 KO H1299 cell lines by CRISPR-Cas9n and reconstitution with Dyn1-EGFP constructs

Genome editing of H1299 cells was performed using a double-nicking strategy to knockout (KO) endogenous dynamin-1. Two pairs of 20-bp-long dynamin-1 sgRNAs (single guide) were designed using the CRISPR design tool available at www.genome-engineering.org/crispr (Ran *et al*, 2013). The guide RNA pairs (+ and − strands) were cloned into a bicistronic expression vector (pX335) containing a human codon-optimized Cas9n and necessary RNA components (Addgene). Top two double nickase "hits" targeting exon 1 of human dynamin-1 were chosen for cloning into pX335 vector. The sgRNA pair (A) for Clone A9 and Clone A19: 5′-TTCCATGCCG CGGTTGCCCATGG-3′ and 5′-ATCTCATCCCGCTGGTCAACCGG-3′ and the sgRNA pair (B) for Clone B22: 5′-CCGGCTGCCGCTAGCGC TCCCGG-3′ and 5′-AGCCATGGGCAACCGCGGCATGG-3′ were used.

The single-guide RNAs (sgRNAs) in the pX335 vector (1 μg each for a sgRNA pair) were mixed with pmaxGFP plasmid (0.2 μg; Lonza) and co-transfected into H1299 cells using lipofectamine 2000 transfection reagent (Life Technologies). Forty-eight hours post-transfection, the cells were trypsinized, washed with PBS and resuspended in PBS containing 2% serum. GFP-positive cells were single-cell sorted by FACS (The Moody Foundation Flow Cytometry Facility, UT Southwestern Medical Center, Dallas, TX) into a 96-well plate format into RPMI containing 5% FBS. Single clones were expanded and screened for dynamin-1 expression by Western blotting using the anti-dynamin-1 rabbit monoclonal antibody (EP772Y, Abcam).

Stable reconstitution with WT Dyn1-EGFP and S774A Dyn1-EGFP fusion proteins in H1299 Dyn1 KO cells (Clone B22) was performed

as previously described (Liu *et al*, 2008). Briefly, WT Dyn1 containing an N-terminal HA tag and C-terminal EGFP fusion protein were cloned into pMIEG3 retroviral vector. Virus was produced in 293T packaging cells and the retroviral supernatant was used to infect H1299 Dyn1 KO cells. Cells were collected 48 h post-infection and FACS sorted for low expression levels based on GFP intensity. The S774A mutation was introduced into the above retroviral vector via site directed mutagenesis and similarly infected and sorted for comparable expression levels.

Supplementary information for this article is available online: http://emboj.embopress.org

Acknowledgements

We are grateful to Gaudenz Danuser for critical contributions and discussions leading to the checkpoint hypothesis. We thank the members of the Schmid and Danuser laboratory for discussions and technical assistance, and Mike Henne and Peter Michaely for critically reading the manuscript. This research was supported by National Institutes of Health grants R01 GM73165 (G.D. and S.L.S.) and MH61345 and GM42455 (to S.L.S.). P-HC was supported by a Taiwan National Science Council Grant 103-2917-I-564-029.

Author contributions

CRR and PHC designed the project, performed the experiments and analyzed the results. CRR and SLS wrote the manuscript. SS generated and validated the H1299 Dyn1 KO and reconstituted cell lines. MM assisted with experiments and provided reagents. FA performed the computational analysis of APPL1 and EEA1 by TIRFM. SLS conceived the project, supervised and directed the research. All authors discussed the results and commented on the manuscript.

Conflict of interest

The authors declare that they have no conflict of interest.

References

Aguet F, Antonescu CN, Mettlen M, Schmid SL, Danuser G (2013) Advances in analysis of low signal-to-noise images link dynamin and AP2 to the functions of an endocytic checkpoint. *Dev Cell* 26: 279 – 291

Clayton EL, Sue N, Smillie KJ, O'Leary T, Bache N, Cheung G, Cole AR, Wyllie DJ, Sutherland C, Robinson PJ, Cousins MA (2010) Dynamin I phosphorylation by GSK3 controls activity-dependent bulk endocytosis of synaptic vesicles. *Nat Neurosci* 13: 845 – 851

Cocucci E, Gaudin R, Kirchhausen T (2014) Dynamin recruitment and membrane scission at the neck of a clathrin-coated pit. *Mol Biol Cell* 25: 3595 – 3609

Damke H, Baba T, Warnock DE, Schmid SL (1994) Induction of mutant dynamin specifically blocks endocytic coated vesicle formation. *J Cell Biol* 127: 915 – 934

Di Fiore PP, von Zastrow M (2014) Endocytosis, signaling, and beyond. *Cold Spring Harb Perspect Biol* 6: a016865

Doyon JB, Zeitler B, Cheng J, Cheng AT, Cherone JM, Santiago Y, Lee AH, Vo TD, Doyon Y, Miller JC, Paschon DE, Zhang L, Rebar EJ, Gregory PD, Urnov FD, Drubin DG (2011) Rapid and efficient clathrin-mediated endocytosis revealed in genome-edited mammalian cells. *Nat Cell Biol* 13: 331 – 337

Ehrlich M, Boll W, Van Oijen A, Hariharan R, Chandran K, Nibert ML, Kirchhausen T (2004) Endocytosis by random initiation and stabilization of clathrin-coated pits. *Cell* 118: 591 – 605

Ferguson SM, Brasnjo G, Hayashi M, Wolfel M, Collesi C, Giovedi S, Raimondi A, Gong LW, Ariel P, Paradise S, O'toole E, Flavell R, Cremona O, Meisenböck G, Ryan TA, De Camilli P (2007) A selective activity-dependent requirement for dynamin 1 in synaptic vesicle endocytosis. *Science* 316: 570 – 574

Ferguson SM, De Camilli P (2012) Dynamin, a membrane-remodelling GTPase. *Nat Rev Mol Cell Biol* 13: 75 – 88

Field MC, Gabernet-Castello C, Dacks JB (2007) Reconstructing the evolution of the endocytic system: insights from genomics and molecular cell biology. *Adv Expt Med Biol* 607: 84 – 96

Forgac M (2007) Vacuolar ATPases: rotary proton pumps in physiology and pathophysiology. *Nature Rev Mol Cell Biol* 8: 917 – 929

Gorvel JP, Chavrier P, Zerial M, Gruenberg J (1991) Rab5 controls early endosome fusion in vitro. *Cell* 64: 915 – 925

Grant BD, Donaldson JG (2009) Pathways and mechanisms of endocytic recycling. *Nat Rev Mol Cell Biol* 10: 597 – 608

Haferlach T, Kohlmann A, Wieczorek L, Basso G, Kronnie GT, Bene MC, De Vos J, Hernandez JM, Hofmann WK, Mills KI, Gilkes A, Chiaretti S, Shurtleff SA, Kipps TJ, Rassenti LZ, Yeoh AE, Papenhaussen PR, Liu WM, Williams PM, Foa R (2010) Clinical utility of microarray-based gene expression profiling in the diagnosis and subclassification of leukemia: report from the International Microarray Innovations in Leukemia Study Group. *J Clin Oncol* 28: 2529 – 2537

Hernandez V.J., Weng J., Ly P., Pompey S., Dong H., Mishra L., Schwarz M., Anderson R.G., Michaely P. (2013). Cavin-3 dictates the balance between ERK and Akt signaling. *eLife* 2: e00905.

Hong Y, Downey T, Eu KW, Koh PK, Cheah PY (2010) A 'metastasis-prone' signature for early-stage mismatch-repair proficient sporadic colorectal cancer patients and its implications for possible therapeutics. *Clin Exp Metastasis* 27: 83 – 90

Huang F, Khvorova A, Marshall W, Sorkin A (2004) Analysis of clathrin-mediated endocytosis of epidermal growth factor receptor by RNA interference. *J Biol Chem* 279: 16657 – 16661

Kasprowicz J, Kuenen S, Swerts J, Miskiewicz K, Verstreken P (2014) Dynamin photoinactivation blocks Clathrin and alpha-adaptin recruitment and induces bulk membrane retrieval. *J Cell Biol* 204: 1141 – 1156

Le Roy C, Wrana JL (2005) Clathrin- and non-clathrin-mediated endocytic regulation of cell signalling. *Nat Rev Mol Cell Biol* 6: 112 – 126

Liberali P, Snijder B, Pelkmans L (2014) A hierarchical map of regulatory genetic interactions in membrane trafficking. *Cell* 157: 1473 – 1487

Liu AP, Aguet F, Danuser G, Schmid SL (2010) Local clustering of transferrin receptors promotes clathrin-coated pit initiation. *J Cell Biol* 191: 1381 – 1393

Liu YW, Neumann S, Ramachandran R, Ferguson SM, Pucadyil TJ, Schmid SL (2011) Differential curvature sensing and generating activities of dynamin isoforms provide opportunities for tissue-specific regulation. *Proc Natl Acad Sci USA* 108: E234 – E242

Liu YW, Su AI, Schmid SL (2012) The evolution of dynamin to regulate clathrin-mediated endocytosis: speculations on the evolutionarily late appearance of dynamin relative to clathrin-mediated endocytosis. *BioEssays* 34: 643 – 647

Liu YW, Surka MC, Schroeter T, Lukiyanchuk V, Schmid SL (2008) Isoform and splice-variant specific functions of dynamin-2 revealed by analysis of conditional knock-out cells. *Mol Biol Cell* 19: 5347 – 5359

Loerke D, Mettlen M, Yarar D, Jaqaman K, Jaqaman H, Danuser G, Schmid SL (2009) Cargo and dynamin regulate clathrin-coated pit maturation. *PLoS Biol* 7: e57

Maxfield FR, McGraw TE (2004) Endocytic recycling. *Nat Rev Mol Cell Biol* 5: 121 – 132

McMahon HT, Boucrot E (2011) Molecular mechanism and physiological functions of clathrin-mediated endocytosis. *Nat Rev Mol Cell Biol* 12: 517 – 533

Mellman I (1996) Endocytosis and molecular sorting. *Ann Rev Cell Dev Biol* 12: 575 – 625

Mellman I, Yarden Y (2013) Endocytosis and cancer. *Cold Spring Harb Perspect Biol* 5: a016949

Mettlen M, Pucadyil T, Ramachandran R, Schmid SL (2009a) Dissecting dynamin's role in clathrin-mediated endocytosis. *Biochem Soc Trans* 37: 1022 – 1026

Mettlen M, Stoeber M, Loerke D, Antonescu CN, Danuser G, Schmid SL (2009b) Endocytic accessory proteins are functionally distinguished by their differential effects on the maturation of clathrin-coated pits. *Mol Biol Cell* 20: 3251 – 3260

Mosesson Y, Mills GB, Yarden Y (2008) Derailed endocytosis: an emerging feature of cancer. *Nat Rev Cancer* 8: 835 – 850

Motley AM, Berg N, Taylor MJ, Sahlender DA, Hirst J, Owen DJ, Robinson MS (2006) Functional analysis of AP-2 alpha and mu2 subunits. *Mol Biol Cell* 17: 5298 – 5308

Palfy M, Remenyi A, Korcsmaros T (2012) Endosomal crosstalk: meeting points for signaling pathways. *Trends Cell Biol* 22: 447 – 456

Platta HW, Stenmark H (2011) Endocytosis and signaling. *Curr Opin Cell Biol* 23: 393 – 403

Ran FA, Hsu PD, Lin CY, Gootenberg JS, Konermann S, Trevino AE, Scott DA, Inoue A, Matoba S, Zhang Y, Zhang F (2013) Double nicking by RNA-guided CRISPR Cas9 for enhanced genome editing specificity. *Cell* 154: 1380 – 1389

Rink J, Ghigo E, Kalaidzidis Y, Zerial M (2005) Rab conversion as a mechanism of progression from early to late endosomes. *Cell* 122: 735 – 749

Schenck A, Goto-Silva L, Collinet C, Rhinn M, Giner A, Habermann B, Brand M, Zerial M (2008) The endosomal protein Appl1 mediates Akt substrate specificity and cell survival in vertebrate development. *Cell* 133: 486 – 497

Schmid EM, McMahon HT (2007) Integrating molecular and network biology to decode endocytosis. *Nature* 448: 883 – 888

Schmid SL, Smythe E (1991) Stage-specific assays for coated pit formation and coated vesicle budding in vitro. *J Cell Biol* 114: 869 – 880

Sever S, Damke H, Schmid SL (2000) Dynamin:GTP controls the formation of constricted coated pits, the rate limiting step in clathrin-mediated endocytosis. *J Cell Biol* 150: 1137 – 1148

Sever S, Muhlberg AB, Schmid SL (1999) Impairment of dynamin's GAP domain stimulates receptor-mediated endocytosis. *Nature* 398: 481 – 486

Smillie KJ, Cousin MA (2011) The role of GSK3 in presynaptic function. *Int J Alzheimer's Dis* 2011: 263673

Sorkin A, von Zastrow M (2009) Endocytosis and signalling: intertwining molecular networks. *Nat Rev Mol Cell Biol* 10: 609 – 622

Taylor MJ, Lampe M, Merrifield CJ (2012) A feedback loop between dynamin and actin recruitment during clathrin-mediated endocytosis. *PLoS Biol* 10: e1001302

Traub LM (2009) Tickets to ride: selecting cargo for clathrin-regulated internalization. *Nat Rev Mol Cell Biol* 10: 583 – 596

Villasenor R., Nonaka H., Del Conte-Zerial P., Kalaidzidis Y., Zerial M. (2015). Regulation of EGFR signal transduction by analogue-to-digital conversion in endosomes. *eLife* 4: e06156

Zoncu R, Perera RM, Balkin DM, Pirruccello M, Toomre D, De Camilli P (2009) A phosphoinositide switch controls the maturation and signaling properties of APPL endosomes. *Cell* 136: 1110 – 1121

